INTERNATIONAL JOURNAL FOR NUMERICAL METHODS IN FLUIDS, VOL. 5, 201–224 (1985)

THE GROUP VELOCITY OF SOME NUMERICAL SCHEMES

B. CATHERS* AND B. A. O'CONNOR†

Department of Civil Engineering, Simon Engineering Laboratories, University of Manchester, Manchester, M13 9PL, U.K.

SUMMARY

The performances of various numerical schemes used to model hyperbolic/parabolic equations have been studied by the calculation of their numerical group velocities. Numerical experiments conducted with one dimensional linear and quadratic Lagrangian finite elements with a Crank–Nicolson finite differencing in time confirm the results of the analysis. The group velocity analysis supplements the well-known amplitude and phase portraits introduced by Leendertse[1] and helps explain the occurrence and behaviour of numerical oscillations in both finite difference and finite element schemes.

KEY WORDS Numerical Group Velocity Fourier Analysis

INTRODUCTION

It is well known that the accuracy of numerical schemes cannot be gauged simply by a truncation error analysis. Indeed, numerical schemes with the same order of accuracy can have widely different behaviours. Von Neumann used a Fourier analysis to investigate the linear stability of a numerical scheme. Leendertse[1] used a Fourier analysis to estimate the accuracy of numerical schemes with regard to amplitude and phase speed errors. Sobey[2] carried out similar analyses on four well tried and proven finite difference schemes. The present work is concerned with the accuracy and behaviour of numerical schemes used in tidal modelling and attempts to explain errors found in them by introducing a Fourier analysis based on the concept of group velocity.

SHALLOW WATER EQUATIONS AND THE TRANSPORT EQUATION

The one-dimensional equations describing tidal motion in estuaries can be written as follows:

$$\frac{\partial u}{\partial t} + u\frac{\partial u}{\partial x} + g\frac{\partial \eta}{\partial x} + g\frac{u|u|}{C_h^2 h} = 0 \tag{1}$$

$$\frac{\partial \eta}{\partial t} + \frac{\partial}{\partial x}(hu) = 0 \tag{2}$$

where u is a cross-sectionally averaged velocity; C_h is the Chezy coefficient ($m^{1/2}/s$); $h = h_0 + \eta$ is the cross-sectionally averaged flow depth relative to mean water level; η is the water surface elevation measured from mean water level and h_0 is the mean water depth. Both equations (1) and (2) reduce to the transport equation (3) when the mean water depth is constant and the non-linear terms neglected.

$$\frac{\partial u}{\partial t} + c\frac{\partial u}{\partial x} = 0 \tag{3}$$

Present addresses: * N.S.W. Department of Public Works, King St, Manly Vale 2093, Australia
† Department of Civil Engineering, University of Liverpool, Liverpool, U.K.

0271–2091/85/03 0201–24$02.40
© 1985 by John Wiley & Sons, Ltd.
Received 1 November 1983
Revised 6 April 1984

where

$$c = \sqrt{(gh_0)} \quad \text{and} \quad u = c\eta/h_0$$

The general solution of equation (3) can be represented by the Fourier series.

$$u = \sum_{m=-\infty}^{\infty} \hat{U}_m e^{i(\omega_m t + \sigma_m x)} \tag{4}$$

where $\hat{U}_m$ is a constant amplitude of the mth component; ω_m is the angular frequency of the mth component and σ_m is the mth wave number component.

Equation (4) describes the physical continuum by an infinite series of progressive waves whose phase and group velocities are identical. This can be shown by considering one component of the wave spectrum, that is,

$$\begin{aligned} u &= \hat{U} e^{i(\omega t + \sigma x)} \\ &= u(t) e^{i\sigma x} \end{aligned} \tag{5}$$

where $u(t)$ is the wave amplitude at time t and subscript m has been dropped for convenience.

The phase velocity of the wave (C_p) is found from the dispersion relationship for the continuum by substituting equation (5) into equation (3), that is

$$\begin{aligned} C_p &= \omega/\sigma \\ &= -c \end{aligned} \tag{6}$$

The group velocity, which represents the speed at which the energy of the spectrum is transmitted, is found by differentiating equation (6), that is,

$$\begin{aligned} C_g &= \frac{\partial \omega}{\partial \sigma} \\ &= -c \end{aligned} \tag{7}$$

Thus, the analytical solution to equation (3) is non-dispersive since all wavelengths propagate at the same phase speed which, in this case, is the same as the group velocity.

FOURIER SERIES ANALYSIS OF A FINITE ELEMENT SOLUTION

Numerical solutions of equation (3) and, by implication, equations (1) and (2), will experience problems when attempting to model the physical continuum. Clearly, numerical schemes can only reproduce a finite number of wave components; the spectrum being truncated for wavelengths less than or equal to $2\Delta x$. The implication is that the numerical spectrum will segregate since both the wave speed and the rate of energy transfer of the numerical waves are different from those of the continuum waves, thereby leading to numerical oscillations.

The dispersive nature of the numerical spectrum can be seen by writing equation (3) in discrete form. Using linear finite elements or, more specifically, a Galerkin finite element method with linear shape functions in space and an implicit finite difference technique in time, yields the following numerical analogue of equation (3):

$$\begin{aligned} &\frac{1}{6}\left\{\left(\frac{U^{n+1} - U^n}{\Delta t}\right)_{j-1} + 4\left(\frac{U^{n+1} - U^n}{\Delta t}\right)_j + \left(\frac{U^{n+1} - U^n}{\Delta t}\right)_{j+1}\right\} + c\theta\left(\frac{U_{j+1} - U_{j-1}}{2\Delta x}\right)^{n+1} \\ &\quad + c(1-\theta)\left(\frac{U_{j+1} - U_{j-1}}{2\Delta x}\right)^{n} = 0 \end{aligned} \tag{8}$$

where j, n are the spatial and temporal grid counters in increments of Δx and Δt, respectively. θ is a time weighting factor ($\theta = \frac{1}{2}$ corresponds to a Crank–Nicolson scheme; $\theta = 2/3$ corresponds to linear shape functions in both space and time; $\theta = 1$ corresponds to a fully-implicit scheme).

Considering only a single numerical Fourier wave component leads to the dispersion relationship by substitution of equation (5) into equation (8), that is

$$\tan\left(\frac{\omega_{\text{num}}\Delta t}{2}\right) = \frac{-\frac{3}{2}\left(\frac{c\Delta t}{\Delta x}\right)\sin(\sigma\Delta x)}{\cos(\sigma\Delta x)+2} \tag{9}$$

where ω_{num} is the angular frequency of the numerical scheme, which is in general complex, but for space and time centred schemes, such as considered here, is real.

Comparison of equations (6) and (9) shows that the numerical system is frequency dispersive, and that the dispersion relation only approaches that of the continuum as Δx, $\Delta t \to 0$. It is this frequency dispersive property of numerical schemes which is the main theme of the present paper.

COMPLEX PROPAGATION FACTOR, EIGENVALUES, AMPLITUDE RATIO AND VELOCITY RATIO

In this section, relationships are established between the various traditional parameters such as propagation factor, amplitude and phase velocity ratios, in terms of both the angular frequency and the eigenvalue. These three factors are often used to assess the accuracy of numerical schemes.

The real and imaginary parts of the angular frequencies will be represented as follows:

$$\textit{discrete system} \quad \omega_{\text{num}} = \Omega_{\text{num}} + \mathrm{i}\nu_{\text{num}} \tag{10}$$

$$\textit{continuum} \quad \omega = \Omega + \mathrm{i}\nu \tag{11}$$

In particular, for equation (3), $\nu = 0$; Ω_{num} is related to the *ever-present* dispersion in a numerical scheme, whereas ν_{num} pertains to the dissipation or attenuation which may or may not be present in a numerical scheme.

The (complex) eigenvalue λ_{num} is the ratio of the amplitude of the computed solution at successive time levels, separated by Δt. The eigenvalue is often relatively accessible and is a convenient parameter when assessing numerical schemes. From equations (5) and (10)

$$\lambda_{\text{num}} = \frac{u(t+\Delta t)}{u(t)} = \mathrm{e}^{\mathrm{i}\omega_{\text{num}}\Delta t} = \mathrm{e}^{-\nu_{\text{num}}\Delta t}\mathrm{e}^{\mathrm{i}\Omega_{\text{num}}\Delta t} \tag{12}$$

Similarly for the analytical case, we can define

$$\begin{aligned}\lambda &= \mathrm{e}^{\mathrm{i}\omega\Delta t} \\ &= \mathrm{e}^{-\nu\Delta t}\mathrm{e}^{\mathrm{i}\Omega\Delta t}\end{aligned} \tag{13}$$

In 1967, Leendertse[1] introduced the now well-known method of assessing the accuracy of a numerical solution to finite difference (or finite element) equations, relative to the analytical solution of the partial differential equations. He defined the complex propagation factor (PF) as the ratio of the numerical wave to the analytical wave after the time taken for the *analytical* wave to traverse one wavelength L, i.e.

$$\text{PF} = \frac{\mathrm{e}^{\mathrm{i}(\omega_{\text{num}}T+\sigma L)}}{\mathrm{e}^{\mathrm{i}(\omega T+\sigma L)}} \tag{14}$$

where T= analytical wave period $= 2\pi/\Omega$. Substitution of equations (10) to (13) into equation (14)

then yields

$$\begin{aligned} \mathrm{PF} &= \mathrm{e}^{-2\pi((\nu_{\mathrm{num}}-\nu)/\Omega)}\mathrm{e}^{\mathrm{i}2\pi(\Omega_{\mathrm{num}}/\Omega-1)} \\ &= \left|\frac{\lambda_{\mathrm{num}}}{\lambda}\right|^{T/\Delta t} \exp\left\{2\pi\mathrm{i}\left[\left(\tan^{-1}\frac{\mathrm{Im}(\lambda_{\mathrm{num}})}{\mathrm{Re}(\lambda_{\mathrm{num}})}\right)\Big/\Omega\Delta t - 1\right]\right\} \\ &= |\mathrm{PF}|\exp\{\mathrm{i}\arg(\mathrm{PF})\} \end{aligned} \tag{15}$$

where Im( ) and Re( ) stand for the imaginary and real parts.

The amplitude ratio (P) equals the amplitude of the computed wave after time T divided by the amplitude of the analytical wave after the same time and equals the modulus of the propagation factor. Thus from equation (15)

$$\begin{aligned} P &= |\mathrm{PF}| \\ &= \mathrm{e}^{-2\pi((\nu_{\mathrm{num}}-\nu)/\Omega)} \\ &= \left|\frac{\lambda_{\mathrm{num}}}{\lambda}\right|^{T/\Delta t} \end{aligned} \tag{16}$$

The velocity ratio (Q) equals the (real) speed of propagation of the computed wave divided by the (real) speed of propagation of the analytical wave and is related to the argument of the propagation factor. Whenever the angular frequencies ω or ω_{num} are complex, it is necessary to take the real part. Thus from equation (15), we have

$$\begin{aligned} Q &= \frac{\Omega_{\mathrm{num}}}{\Omega} \\ &= \frac{\arg(\mathrm{PF})}{2\pi} + 1 \\ &= \frac{\tan^{-1}[\mathrm{Im}(\lambda_{\mathrm{num}})/\mathrm{Re}(\lambda_{\mathrm{num}})]}{\Omega\Delta t} \end{aligned} \tag{17}$$

Thus the parameters λ_{num}, P and Q are used to assess and characterize the stability and behaviour of a numerical scheme. In particular, we note from equation (12) that a scheme is neutrally stable if $|\lambda_{\mathrm{num}}| = 1$; that is if $\nu_{\mathrm{num}} = 0$; stable and dissipative if $|\lambda_{\mathrm{num}}| \leqslant 1$, that is $\nu_{\mathrm{num}} > 0$; unstable if $|\lambda_{\mathrm{num}}| > 1$, which implies $\nu_{\mathrm{num}} < 0$.

With regard to the propagation factor, it is evident from equation (15) that a numerical scheme has a unit amplitude ratio if $\nu_{\mathrm{num}} = \nu$. More specifically, for space centred schemes, $\nu_{\mathrm{num}} = 0$ whenever $\nu = 0$ and this means that $P = 1$, implying that there are no amplitude errors for any wavelength.

Unlike the amplitude ratio, the phase velocity ratio is not normally unity for all wavelengths. Equation (17) indicates whether the phase errors are lagging or leading depending on the sign of arg (PF). This equation also indicates that a wavelength with a real eigenvalue has a zero phase velocity in the numerical scheme.

GROUP VELOCITY RATIO

It is the intention of this paper to show that the behaviour of a numerical scheme, which is traditionally characterized by the amplitude and phase portraits, can be supplemented by a group velocity portrait.

In 1976, Grotjahn and O'Brien[3] compared the group velocity ratios for the explicit leap-frog and

the implicit Crank–Nicolson finite difference operators applied to equation (3) at Courant numbers of 0·5, 0·99 and also 10 for the implicit scheme. They showed that for wavelengths less than $4\Delta x$, the numerical group velocity was in fact negative. They also compared the group velocities of the 2nd and 4th order leap-frog finite difference schemes. Their work has been extended in the present paper and the expressions for the numerical group velocity will now be derived for the 1-D linearized finite-amplitude shallow water equations which here include the convective acceleration, friction and diffusion terms.

In order to produce the group velocity portraits, it is necessary to linearize equations (1) and (2) and introduce a horizontal momentum transfer term which is often included in numerical models to control numerical stability. These equations then take the form

$$\frac{\partial u}{\partial t} + U_0 \frac{\partial u}{\partial x} + g\frac{\partial \eta}{\partial x} + ku - D_0 \frac{\partial^2 u}{\partial x^2} = 0 \tag{18}$$

$$\frac{\partial \eta}{\partial t} + h_0 \frac{\partial u}{\partial x} + U_0 \frac{\partial \eta}{\partial x} = 0 \tag{19}$$

where U_0 is a constant, unperturbed velocity, $k = g|U_0|/(C_h^2 h_0)$, D_0 is a horizontal momentum transfer coefficient and it is assumed that $\partial\eta/\partial x \gg \partial h_0/\partial x$.

Continuum group velocity

Substitution of

$$U = \hat{U} e^{i(\omega t + \sigma x)} \tag{20}$$

and

$$\eta = \hat{\eta} e^{i(\omega t + \sigma x)} \tag{21}$$

into equations (18) and (19) yields

$$i(\omega + \sigma U_0)\hat{\eta} + i\sigma h_0 \hat{U} = 0 \tag{22}$$

$$i\sigma g\hat{\eta} + [i(\omega + \sigma U_0) + k + \sigma^2 D_0]\hat{U} = 0 \tag{23}$$

For non-trivial $\hat{U}$, $\hat{\eta}$, the solution of equations (22) and (23) yields the dispersion relation for the continuum, that is

$$\omega^{\pm} = -\sigma U_0 + i\frac{(k + \sigma^2 D_0)}{2} \mp \sqrt{\left[(\sigma c)^2 - \left(\frac{k + \sigma^2 D_0}{2}\right)^2\right]} \tag{24}$$

where ω^+, ω^- are the angular velocities corresponding to waves propagating in the $+x$, $-x$ directions, respectively.

Differentiating equation (24) with respect to σ yields the continuum group velocity

$$C_g^{\pm} = -U_0 + i(\sigma D_0) \mp \frac{c^2\sigma - \sigma D_0\left(\frac{k + \sigma^2 D_0}{2}\right)}{\sqrt{\left[(\sigma c)^2 - \left(\frac{k + \sigma^2 D_0}{2}\right)^2\right]}} \tag{25}$$

It is convenient for future analysis to work in terms of dimensionless numbers, and therefore the following parameters are introduced:

$$\mathbb{C} = \frac{c\Delta t}{\Delta x} \qquad \text{(Courant number)} \tag{26a}$$

$$\mathbb{F} = \frac{U_0}{c} \qquad \text{(Froude number)} \tag{26b}$$

$$\mathbb{D} = \frac{D_0 \Delta t}{\Delta x^2} \qquad \text{(diffusion number)} \tag{26c}$$

$$\mathbb{K} = k\Delta t \qquad \text{(friction number)} \tag{26d}$$

$$\gamma = \sigma \Delta x \qquad \text{(dimensionless wavenumber)} \tag{26e}$$

$$= \frac{2\pi}{N_x}$$

$$N_x = L/\Delta x \qquad \text{(dimensionless wavelength)} \tag{26f}$$

Substituting equations (26) into equations (24) and (25) and taking the real parts, gives the results:

$$\mathrm{Re}(\omega^{\pm}\Delta t) = \gamma\mathbb{C}\left\{ -\mathbb{F} \mp \sqrt{\left[1 - \left(\frac{\mathbb{K} + \gamma^2\mathbb{D}}{2\gamma\mathbb{C}}\right)^2\right]}\right\} \tag{27}$$

$$\mathrm{Re}(C_g^{\pm}\sigma\Delta t) = \gamma\mathbb{C}\left\{ -\mathbb{F} \mp \frac{\gamma\mathbb{C} - \dfrac{\mathbb{D}\gamma}{\mathbb{C}}\left(\dfrac{\mathbb{K} + \gamma^2\mathbb{D}}{2}\right)}{\sqrt{\left[(\gamma\mathbb{C})^2 - \left(\dfrac{\mathbb{K} + \gamma^2\mathbb{D}}{2}\right)^2\right]}}\right\} \tag{28}$$

The real parts were taken above since this is the physical quantity of interest when finding the phase and group velocities. It needs to be added that when $\mathbb{K}$ or $\mathbb{D}$ are non-zero, the system is non-conservative and the concept of group velocity loses it utility as energy losses become more significant. A wave system has two aspects, namely kinematic and dynamic. The group velocity is a kinematic concept. Broer[4] has shown that in linear conservative systems, these two velocities are equal. In non-conservative systems they are of less value and in non-linear systems there can be more than one group velocity. Whitham[5] has shown that for finite amplitude waves, the linear group velocity splits into two amplitude dependent group velocities. Therefore, in the work that follows the conclusions reached should only be applied to the case of $\mathbb{K} = \mathbb{D} = \mathbb{F} = 0$ with the additional requirement that $|\lambda_{\mathrm{num}}| = 1$ in the discrete system. Nevertheless, the effect of non-zero $\mathbb{K}$, $\mathbb{D}$, $\mathbb{F}$, and $|\lambda_{\mathrm{num}}| \neq 1$ will be investigated so that indicators can be given on the behaviour of non-conservative systems. If $\mathbb{K} = \mathbb{D} = 0$, equations (27) and (28) show that the continuum system is non-dispersive in terms of both energy and amplitude.

Numerical group velocity

In general, the eigenvalue (or amplification factor) of a numerical scheme is more accessible than ω_{num} and so the expression for the numerical group velocity ($C_{g_{\mathrm{num}}}$) is derived in terms of the eigenvalue. From equation (9) we can find the inverse expression with ω_{num} in terms of λ_{num}, that is

$$\omega_{\mathrm{num}}\Delta t = \tan^{-1}\left[\frac{\mathrm{Im}(\lambda_{\mathrm{num}})}{\mathrm{Re}(\lambda_{\mathrm{num}})}\right] - \mathrm{i}\ln\lambda_{\mathrm{num}} \tag{29}$$

Since only the real part of the numerical group velocity is of physical interest, only the real part of

equation (29) is wanted.

$$\mathrm{Re}(\omega_{\mathrm{num}}\Delta t) = \tan^{-1}\left[\frac{\mathrm{Im}(\lambda_{\mathrm{num}})}{\mathrm{Re}(\lambda_{\mathrm{num}})}\right] \tag{30}$$

Differentiating equation (30) with respect to σ and incorporating equation (26) produces the following result:

$$\mathrm{Re}(C_{g_{\mathrm{num}}}\sigma\Delta t) = \frac{\gamma}{|\lambda_{\mathrm{num}}|^2}\left\{\mathrm{Re}(\lambda_{\mathrm{num}})\frac{\partial}{\partial\gamma}[\mathrm{Im}(\lambda_{\mathrm{num}})] - \mathrm{Im}(\lambda_{\mathrm{num}})\frac{\partial}{\partial\gamma}[\mathrm{Re}(\lambda_{\mathrm{num}})]\right\} \tag{31}$$

In the special cases of those numerical schemes with $|\lambda_{\mathrm{num}}| = 1$, equation (31) simplifies to

$$\mathrm{Re}(C_{g_{\mathrm{num}}}\sigma\Delta t) = \frac{-\gamma}{\mathrm{Im}(\lambda_{\mathrm{num}})}\frac{\partial}{\partial\gamma}[\mathrm{Re}(\lambda_{\mathrm{num}})] \tag{32}$$

We now introduce the group velocity ratio, R = (group velocity of the computed wave)/(group velocity of the continuum wave) where it is understood that we are only dealing with the real parts. Using equation (31), R becomes

$$R = \left(\frac{\partial\Omega_{\mathrm{num}}}{\partial\sigma}\right)\Big/\left(\frac{\partial\Omega}{\partial\sigma}\right) = \frac{\gamma\left\{\mathrm{Re}(\lambda_{\mathrm{num}})\frac{\partial}{\partial\gamma}[\mathrm{Im}(\lambda_{\mathrm{num}})] - \mathrm{Im}(\lambda_{\mathrm{num}})\frac{\partial}{\partial\gamma}[\mathrm{Re}(\lambda_{\mathrm{num}})]\right\}}{|\lambda_{\mathrm{num}}|^2\mathrm{Re}(C_g\sigma\Delta t)} \tag{33}$$

and if $|\lambda_{\mathrm{num}}| = 1$, equation (33) simplifies to

$$R = \frac{-\gamma\frac{\partial}{\partial\gamma}[\mathrm{Re}(\lambda_{\mathrm{num}})]}{\mathrm{Im}(\lambda_{\mathrm{num}})\mathrm{Re}(C_g\sigma\Delta t)} \tag{34}$$

Thus for any particular numerical scheme applied to the shallow water equations or the transport equation, an expression for the eigenvalue(s) together with equation (28) will define the group velocity ratio. Equations (33) or (34) thus enable the group velocity ratio (R) to be deduced.

Linear finite element scheme

Application of the Galerkin finite element technique to equations (18) and (19) with linear shape functions yields the following equations after integrating the diffusion term by parts:

$$\begin{aligned}
&\frac{1}{6}\left\{\left(\frac{u^{n+1}-u^n}{\Delta t}\right)_{j-1} + 4\left(\frac{u^{n+1}-u^n}{\Delta t}\right)_j + \left(\frac{u^{n+1}-u^n}{\Delta t}\right)_{j+1}\right\} + \theta U_0\left(\frac{u_{j+1}-u_{j-1}}{2\Delta x}\right)^{n+1} \\
&+ (1-\theta)U_0\left(\frac{u_{j+1}-u_{j-1}}{2\Delta x}\right)^{n} + \frac{\theta k}{6}(u_{j-1}+4u_j+u_{j+1})^{n+1} + \frac{(1-\theta)k}{6}(u_{j-1}+4u_j+u_{j+1})^{n} \\
&+ \theta g\left(\frac{\eta_{j+1}-\eta_{j-1}}{2\Delta x}\right)^{n+1} + (1-\theta)g\left(\frac{\eta_{j+1}-\eta_{j-1}}{2\Delta x}\right)^{n} - \theta D_0\left(\frac{u_{j+1}-2u_j+u_{j-1}}{\Delta x^2}\right)^{n+1} \\
&- (1-\theta)D_0\left(\frac{u_{j+1}-2u_j+u_{j-1}}{\Delta x^2}\right)^{n} = 0
\end{aligned} \tag{35}$$

$$\begin{aligned}
&\frac{1}{6}\left\{\left(\frac{\eta^{n+1}-\eta^n}{\Delta t}\right)_{j-1} + 4\left(\frac{\eta^{n+1}-\eta^n}{\Delta t}\right)_j + \left(\frac{\eta^{n+1}-\eta^n}{\Delta t}\right)_{j+1}\right\} + \theta h_0\left(\frac{u_{j+1}-u_{j-1}}{2\Delta x}\right)^{n+1} \\
&+ (1-\theta)h_0\left(\frac{u_{j+1}-u_{j-1}}{2\Delta x}\right)^{n} + \theta U_0\left(\frac{\eta_{j+1}-\eta_{j-1}}{2\Delta x}\right)^{n+1} + (1-\theta)U_0\left(\frac{\eta_{j+1}-\eta_{j-1}}{2\Delta x}\right)^{n} = 0
\end{aligned} \tag{36}$$

Substitution of equations (20), (21) and (26) into equations (35) and (36) and elimination of $\hat{U}$ and $\hat{\eta}$ gives an expression for λ_{num} as follows:

$$\lambda^{\pm}_{\text{num}} = 1 - \left\{ \frac{K - \theta(\mathbb{F}E)^2 + \theta E^2 + \mathrm{i}[\mathbb{F}E(1 + 2\theta K) \pm \sqrt{(E^2 - K^2)}]}{1 + 2\theta K - (\theta \mathbb{F}E)^2 + (\theta E)^2 + 2\mathrm{i}\theta \mathbb{F}E(1 + \theta K)} \right\} \tag{37}$$

Where

$$K = \frac{\mathbb{K}}{2} - 3\mathbb{D}\left(\frac{\cos\gamma - 1}{\cos\gamma + 2}\right)$$

and

$$E = \frac{3\mathbb{C}\sin\gamma}{\cos\gamma + 2}$$

The numerical group velocity ratio for the linear finite element scheme is then found by applying equation (33). These calculations are long but trivial and will not be repeated here—but they do permit one to examine the effects of variations in $\mathbb{C}$, θ, $\mathbb{F}$, $\mathbb{K}$ and $\mathbb{D}$ on the group velocity. Typical results showing the effect of Courant number, time centring and Froude number are shown in Figures 1 to 3 where R is plotted against the dimensionless wavelength, N_x.

The most striking point about Figure 1 is that for $2\Delta x$ wavelengths, the numerical group velocity is not only in the opposite direction to that which it should be, but is also three times too fast. Negative group velocities can be a reality and have been reported in connection with waves in a rotating fluid—but here they only go to show the poor performance of the finite element scheme in modelling the group velocity of $2\Delta x$ wavelengths. It is also noteworthy that the $3\Delta x$ wavelengths have a zero group velocity and that the numerical group velocity only matches the analytical group velocity with any degree of success for the longer waves. Clearly, the wavelength at which better

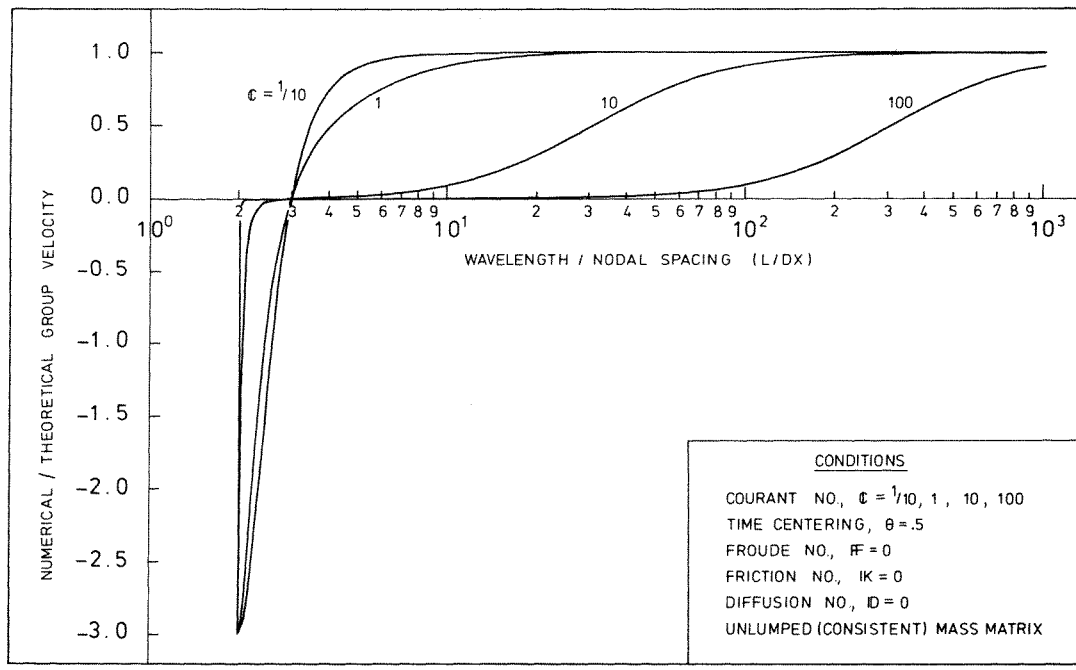

Figure 1. Group velocity portraits of the Crank–Nicolson linear finite element scheme applied to the shallow water equations: effect of Courant number

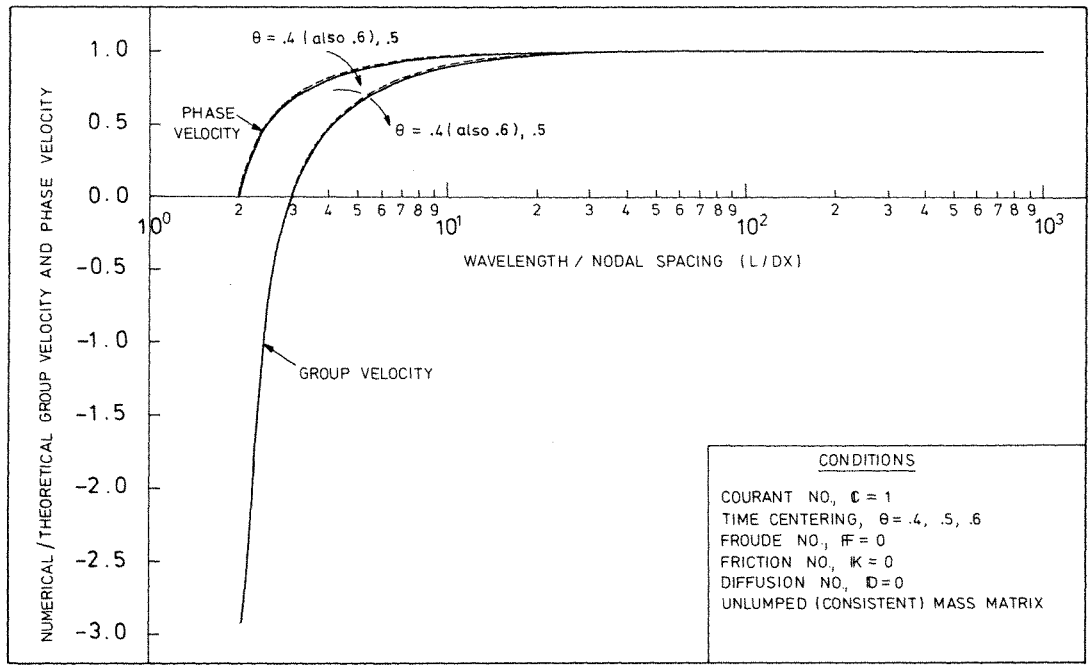

Figure 2. Group and phase velocity portraits of the linear finite element scheme applied to the shallow water equations: effect of time centring

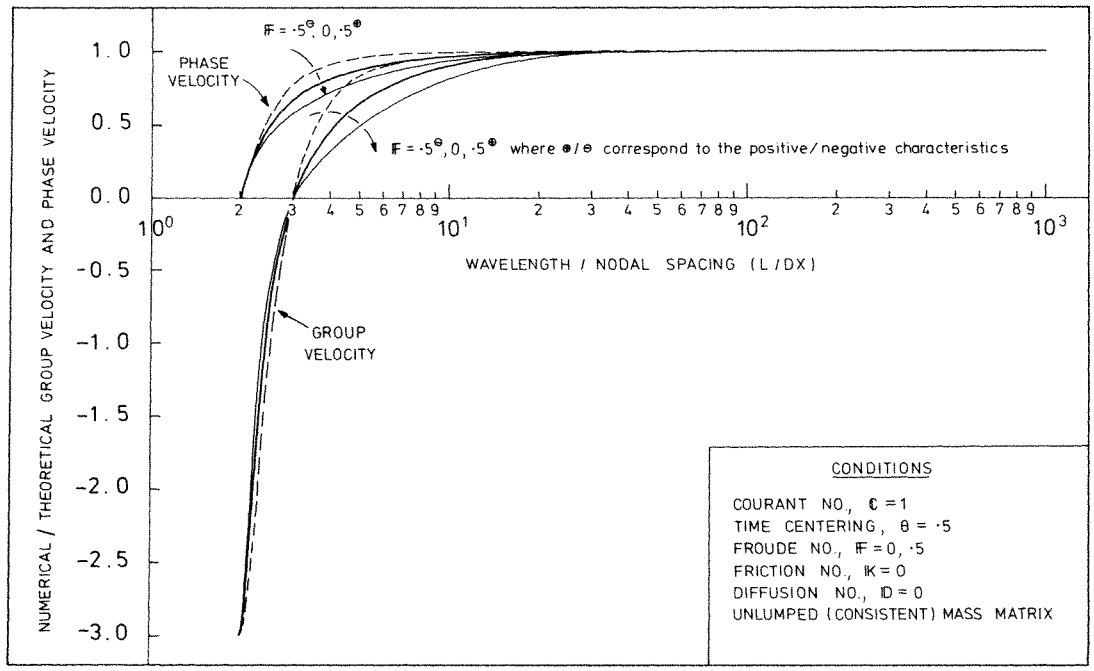

Figure 3. Group and phase velocity portraits of the Crank–Nicolson linear finite element scheme applied to the shallow water equations; effect of Froude number

performance is achieved is very dependent upon the value of the Courant number. The higher the Courant number, the less satisfactory is the performance of the linear elements with regard to both the group and phase velocities.

Figure 2 shows that the group velocity, like the phase velocity, is little influenced by variations in the time centring (θ), especially for the longer waves. Figure 3 shows that a non-zero Froude number introduces anisotropy into the numerical system as the behaviours of the upstream and downstream travelling waves diverge. Relative to the continuum wave, the numerical group velocity of a downstream travelling wave is slower than that for an upstream travelling wave for wavelengths greater than $3\Delta x$. The situation is reversed for wavelengths less than $3\Delta x$. For the phase velocity, however, the numerical phase velocity of a wave heading downstream relative to the corresponding continuum wave is less than that for a wave moving upstream at all wavelengths.

THE NUMERICAL PHASE VELOCITY AND GROUP VELOCITY PUT INTO PERSPECTIVE

The special case of Crank–Nicolson (i.e. $\theta = \frac{1}{2}$) finite elements with $\mathbb{K} = \mathbb{F} = \mathbb{D} = 0$ will now be examined. Under these conditions, the expressions obtained for λ_{num}, P, Q and R which relate to equations (1) and (2) are the same as those obtained for equation (3). Consequently, in this section, the discussion and numerical experiments which follow are made in the context of modelling the transport equation (3) by its linear finite element analogue, equation (8).
Equation (37) can thus be simplified to

$$\lambda^{\pm}_{\text{num}} = \frac{1 \mp \mathrm{i}(E/2)}{1 \pm \mathrm{i}(E/2)} \tag{38}$$

where the $+/-$ correspond to waves travelling downstream/upstream, respectively.

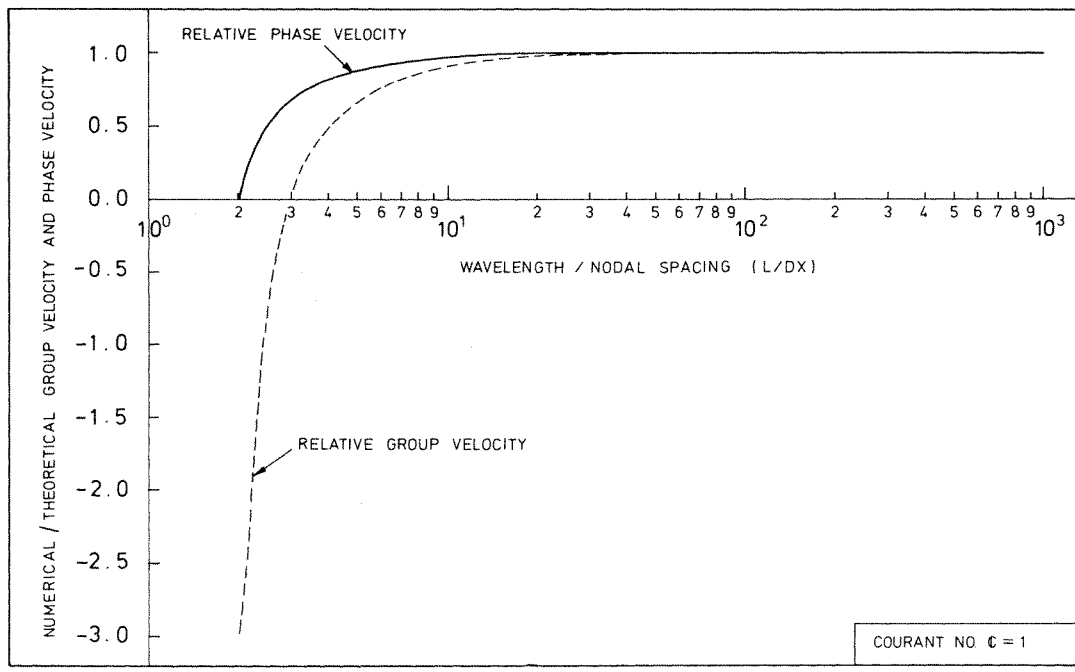

Figure 4. Group and phase velocity portraits for the Crank–Nicolson finite element scheme applied to the shallow water equations

Equation (16) gives

$$P = 1 \tag{39}$$

and equation (17) gives

$$Q = \frac{2\tan^{-1}\left[\dfrac{\frac{3}{2}\mathbb{C}\sin\gamma}{\cos\gamma + 2}\right]}{\gamma\mathbb{C}} \tag{40}$$

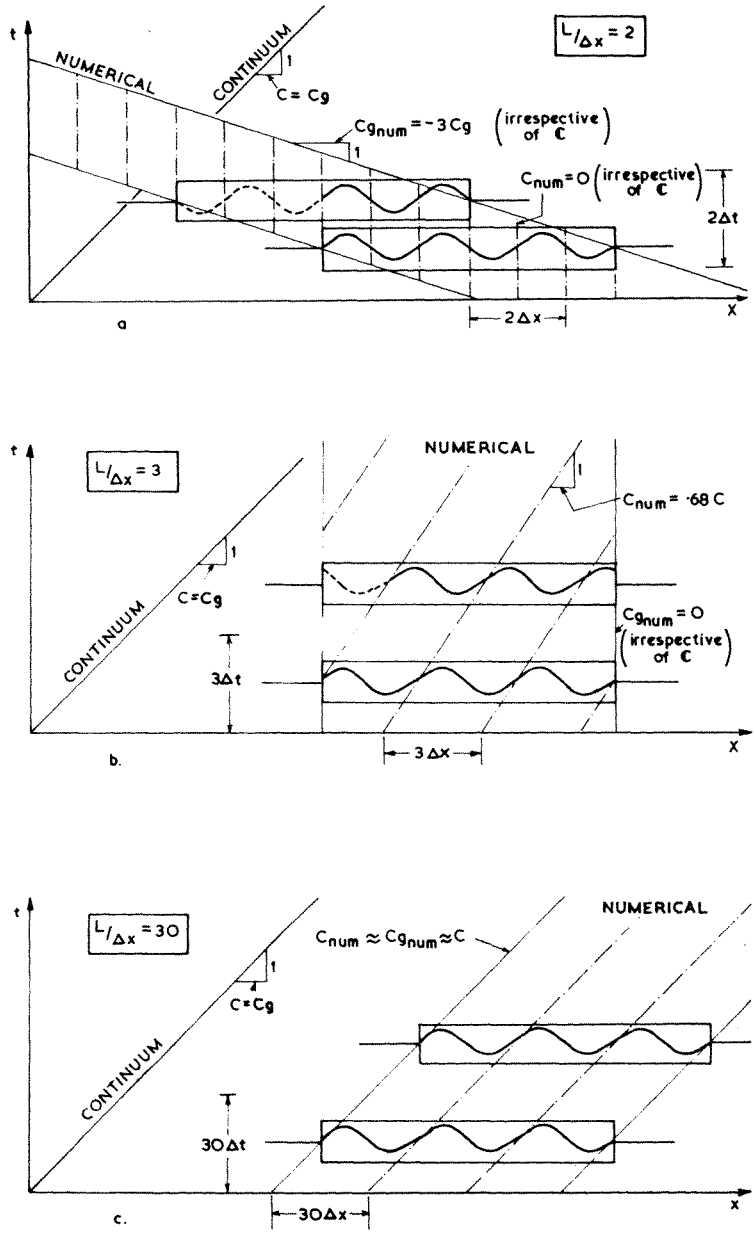

Figure 5. Schematics for the evolution of a wave packet, comprised of various wavelengths ($L/\Delta x = 2, 3, 30$) for the Crank–Nicolson finite element scheme at Courant number $\mathbb{C} = 1$ (dashed sections denote newly-emerging waves)

Since $|\lambda_{num}| = 1$ application of equation (34) results in

$$R = \frac{3(1 + 2\cos\gamma)}{(\cos\gamma + 2)^2 + (\frac{3}{2}\mathbb{C}\sin\gamma)^2} \tag{41}$$

Thus for these conditions, the Crank–Nicolson linear finite element scheme has no amplitude errors (see equation (39)) but it does have errors in both the phase velocity (equation (40)) and the group velocity (equation (41)). Figure 4 shows results for a Courant number equal to 1 and $\theta = \frac{1}{2}$.

It can be seen that at $L = 2\Delta x$, the individual waves are stationary, but the group moves backward at a speed of $-3\sqrt{(gh_0)}$. The situation is depicted in Figure 5(a) which shows that as the group moves backwards at a rate of 3 times the shallow water wave speed, new waves form at the upstream edge of the wave group while existing waves at the downstream edge of the wave group disappear. For comparison, the continuum situation is depicted by the single characteristic line which emanates from the origin.

At $L = 3\Delta x$, the individual waves within a stationary wave group propagate forward at a velocity of about 68 per cent of the continuum speed ($0{\cdot}68\sqrt{(gh_0)}$). This is represented in Figure 5(b) where the vertical band corresponds to the stationary wave group. The sloping characteristics within the band represent the progress of the individual waves.

At $L = 30\Delta x$, the individual waves propagate forward at almost the correct speed (99·6 per cent) while the wave group moves forward at a marginally slower rate (98·9 per cent)—see Figure 5(c).

In the continuum case, both the individual waves and the wave group propagate forward at $\sqrt{(gh_0)}$ for all wavelengths.

NUMERICAL EXPERIMENTS

The behaviour of the Crank–Nicolson linear finite element scheme, as predicted by the analysis, is quite surprising and so a number of numerical experiments were conducted to check their validity.

The experiments were performed by first synthesizing a wave group of about 10 waves with constant amplitude and wavelength ($2\Delta x$). Outside the wave group, the dependent variable was set to zero, thereby completing the specification of the initial conditions. The experiments were then repeated for $4\Delta x$ and $8\Delta x$ wavelengths and at several values of Courant number.

In order to keep the experiments as simple as possible and facilitate the interpretation, the Crank–Nicolson linear finite element version of equation (3), was used rather than equations (18) and (19). This meant that there was only one characteristic in the system, (instead of two) which represented the propagation of disturbances in the $+x$ direction or from left to right in Figures 6–9.

Figure 6 shows how a wave group consisting of $2\Delta x$ waves evolved with time at a Courant number equal to 1. The location of the wave packet is predicted quite well by the analysis, is well outside the continuum location for that wave packet and its shape seems to be approaching that of a Gaussian wave packet. The initial profile is not one of constant form. Since in a dispersive system, only monochromatic waves can have constant form, a Fourier decomposition of the initial conditions in Figure 6 would show that wavelengths other than $2\Delta x$ waves were present at the start of the experiments.

A similar degree of fit between the analysis and experiment was also found for the $4\Delta x$ (not shown) and $8\Delta x$ waves. In the latter case, however, the behaviour of the numerical scheme was found to approach that of the theory so that the continuum and discrete system locations of the wave packet are closer than for the shorter wavelength cases, see Figure 7.

The experiments were repeated at Courant numbers of 1/5 and 5. The results for $\mathbb{C} = 1/5$ were quite similar to those at $\mathbb{C} = 1$, discussed above, but at $\mathbb{C} = 5$, the results took on a more qualitative nature as shown in Figure 8 for $2\Delta x$ waves. The wave packet is seen to be longer than that at the

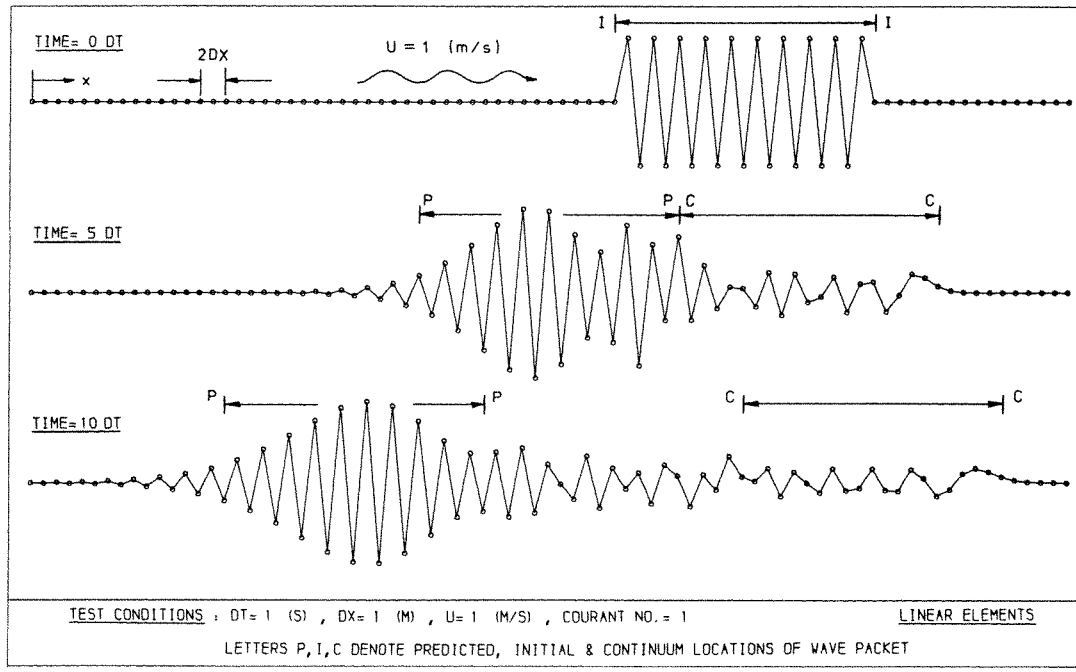

Figure 6. Time evolution of a wave packet made up of waves of wavelength $L = 2\Delta x$

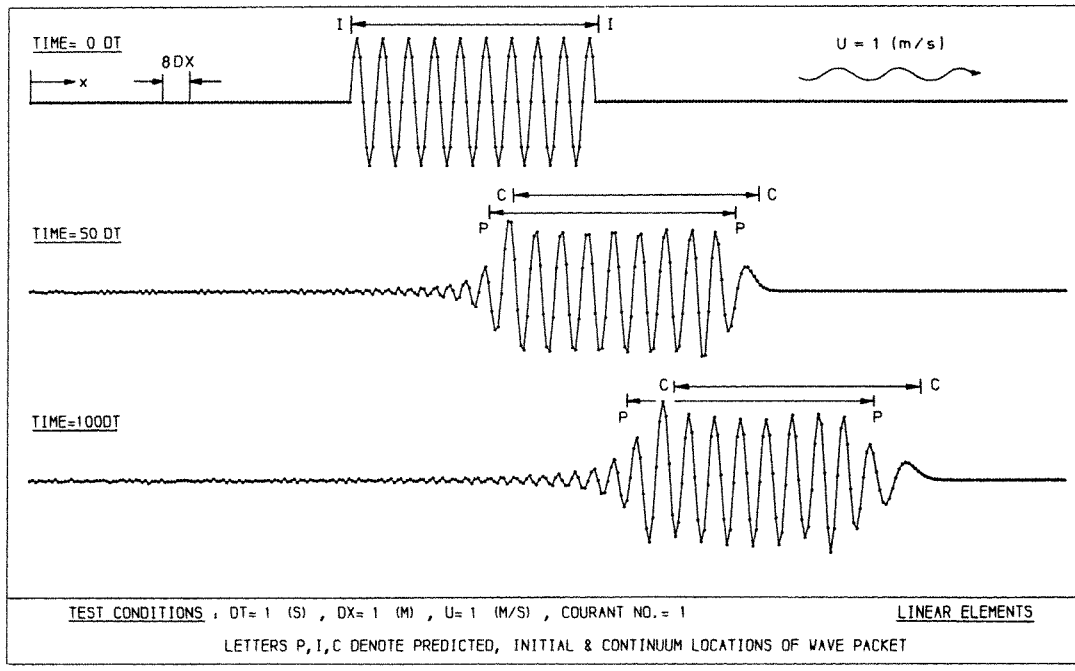

Figure 7. Time evolution of a wave packet made up of waves of wavelength $L = 8\Delta x$

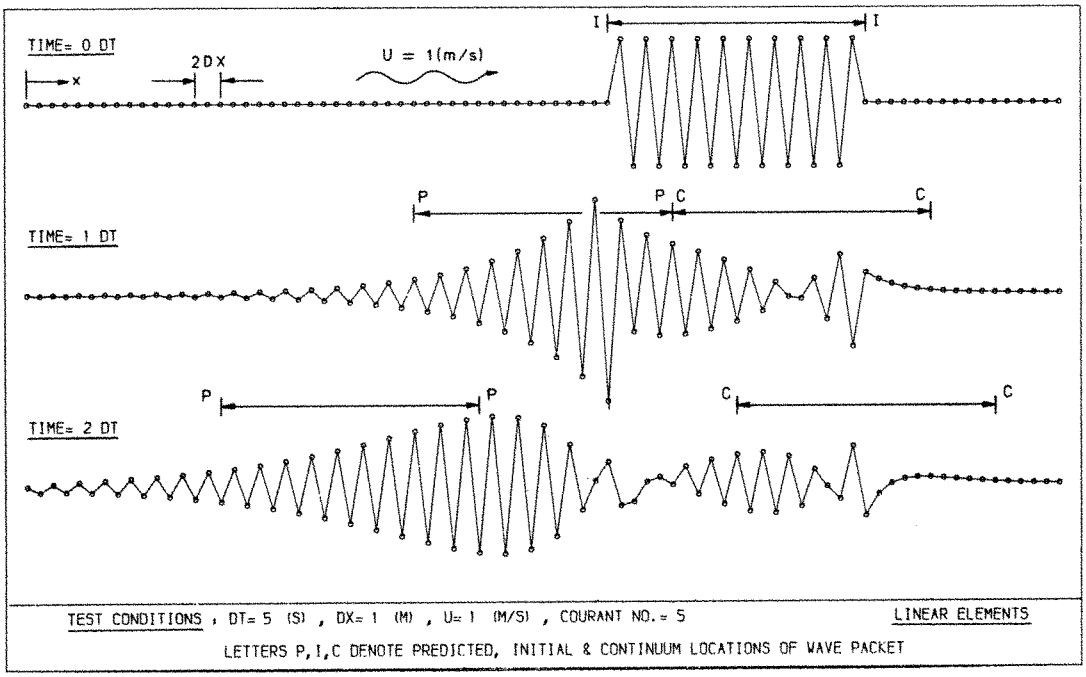

Figure 8. Time evolution of a wave packet made up of waves of wavelength $L = 2\Delta x$

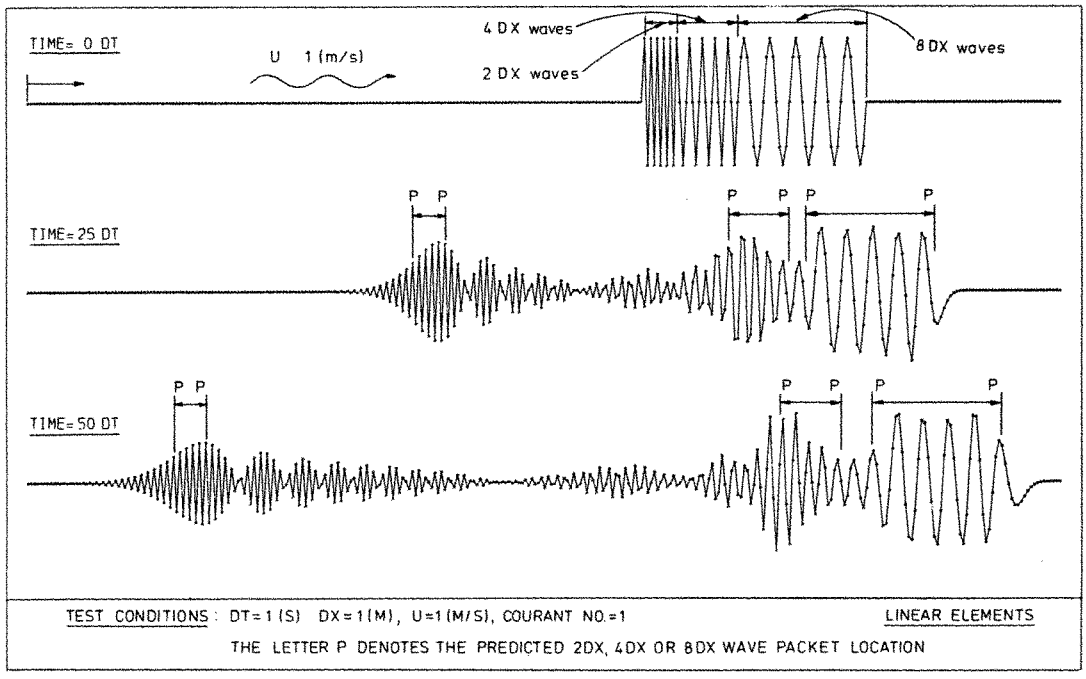

Figure 9. Time evolution of a composite wave packet made up of $2\Delta x$, $4\Delta x$ and $8\Delta x$ waves

lower Courant number of 1 and seems to have broken down into two wave packets, a phenomenon that was also noticed in some later tests. Even after only two time steps, the wave packet is longer at $\mathbb{C} = 5$ because of the greater amount of dispersion present at higher Courant numbers. The centroid of the larger wave packet is also seen to be only just contained between the predicted limits of the wave group. Thus the group velocity predicted by the analysis at $\mathbb{C} = 5$ for $L = 2\Delta x$ waves seems to be underestimated.

Finally, one more experiment was carried out consisting of a composite initial wave packet at $\mathbb{C} = 1$. This consisted contiguously of $2\Delta x$, $4\Delta x$, and $8\Delta x$ waves from the upstream and downstream ends as shown in Figure 9. The analysis predicted that the $2\Delta x$ wave portion would move to the left at a speed of $-3\sqrt{(gh_0)}$, the $4\Delta x$ portion would move to the right at $0{\cdot}480\sqrt{(gh_0)}$ and the $8\Delta x$ portion would move to the right at $0{\cdot}989\sqrt{(gh_0)}$.

The results show (Figure 9) that after 50 time steps the $2\Delta x$ portion has a main wave packet followed by a series of 9 progressively smaller ones. Next comes a long low amplitude wave packet where the waves are between $2\Delta x$ and $4\Delta x$. The next two wave packets are larger and easily discernible as the $4\Delta x$ and $8\Delta x$ contributions. Similar results were found for a composite wave packet composed of $4\Delta x$ waves on the upstream side, followed by $2\Delta x$ waves on the downstream side,[6] although in this case the two wave groups passed through each other. This last test highlights the very different behaviour of the numerical scheme at the various wavelengths and shows that the linear group velocity analysis provides a good first order representation of the behaviour of the numerical solution.

Quadratic elements

Each quadratic element in the one dimensional Lagrange family has two end nodes and one midside node. Applying the Galerkin process with the quadratic shape functions and the same time differencing as was used for the earlier linear element tests, we obtain two equations when modelling the transport equation (3). The end nodes and mid-side nodes have different connectivities and are therefore approximated differently, giving rise to two equations types: one for a typical end node and the other for a typical midside node.

For an end node at $j\Delta x$, equation (3) becomes

$$\frac{1}{10}\left\{-\left(\frac{u^{n+1}-u^n}{\Delta t}\right)_{j-2}+2\left(\frac{u^{n+1}-u^n}{\Delta t}\right)_{j-1}+8\left(\frac{u^{n+1}-u^n}{\Delta t}\right)_j\right.$$
$$\left.+2\left(\frac{u^{n+1}-u^n}{\Delta t}\right)_{j+1}-\left(\frac{u^{n+1}-u^n}{\Delta t}\right)_{j+2}\right\}+\theta c\left(\frac{u_{j-2}-4u_{j-1}+4u_{j+1}-u_{j+2}}{4\Delta x}\right)^{n+1}$$
$$+(1-\theta)c\left(\frac{u_{j-2}-4u_{j-1}+4u_{j+1}-u_{j+2}}{4\Delta x}\right)^{n}=0 \tag{42}$$

For the mid-side node at $(j-1)\Delta x$, the corresponding equation is

$$\frac{1}{10}\left\{\left(\frac{u^{n+1}-u^n}{\Delta t}\right)_{j-2}+8\left(\frac{u^{n+1}-u^n}{\Delta t}\right)_{j-1}+\left(\frac{u^{n+1}-u^n}{\Delta t}\right)_j\right\}$$
$$+\theta c\left(\frac{u_j-u_{j-2}}{2\Delta x}\right)^{n+1}+(1-\theta)c\left(\frac{u_j-u_{j-2}}{2\Delta x}\right)^{n}=0 \tag{43}$$

By making substitutions of the form of equation (5) for both node types we obtain a pair of

simultaneous equations which yield two eigenvalues.

$$\lambda_{\text{num}}^{+/\text{sp}} = \frac{(\cos 2\gamma - 3) - 5\theta(1-\theta)\mathbb{C}^2(\cos 2\gamma - 1) - 2i(1-2\theta)\mathbb{C}\sin 2\gamma \pm 2i\mathbb{C}\sin\gamma\sqrt{(10-\cos^2\gamma)}}{(\cos 2\gamma - 3) + 5\theta^2\mathbb{C}^2(\cos 2\gamma - 1) + 4i\theta\mathbb{C}\sin 2\gamma} \tag{44}$$

where the superscript 'sp' stands for the spurious computational mode that arises because of the two different node types. If $\theta = \frac{1}{2}$, then $|\lambda_{\text{num}}^{+/\text{sp}}| = 1$. Thus the double root for the eigenvalue admits a mechanism for the spurious propagation of waves.

Application of equations (16) and (17) to equation (44) yields the performance curves for the scheme. A particular example is presented in Figure 10 for $\theta = 0{\cdot}6$ and $\mathbb{C} = 1/10$ and 10.

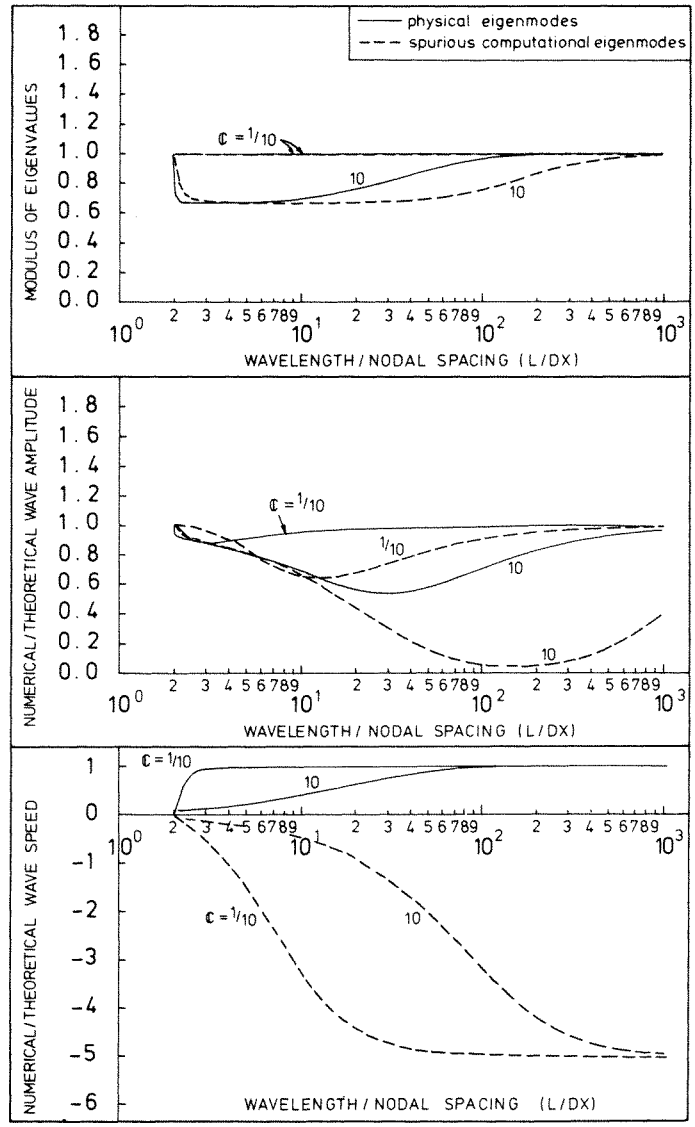

Figure 10. Stability, amplitude and phase velocity portraits of quadratic finite elements: effect of Courant number ($\mathbb{C}$). *Conditions*: $\mathbb{C} = 1/10$, 10; $\theta = 0{\cdot}6$

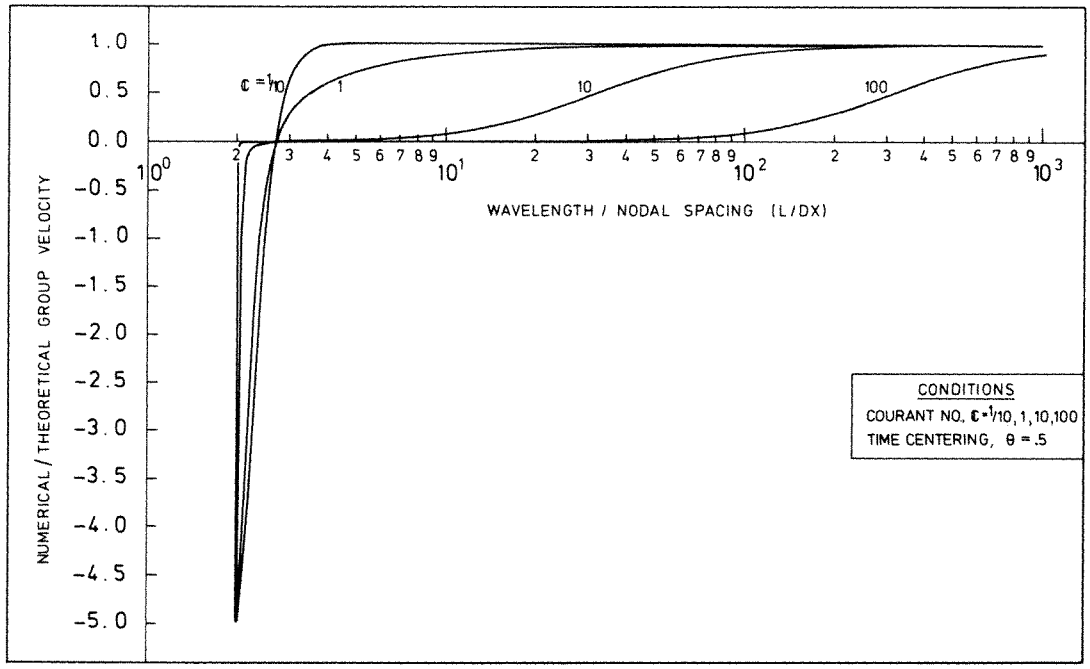

Figure 11. Group velocity portraits for the physical eigenmodes of Crank–Nicolson quadratic elements applied to the shallow water equations: effect of Courant number

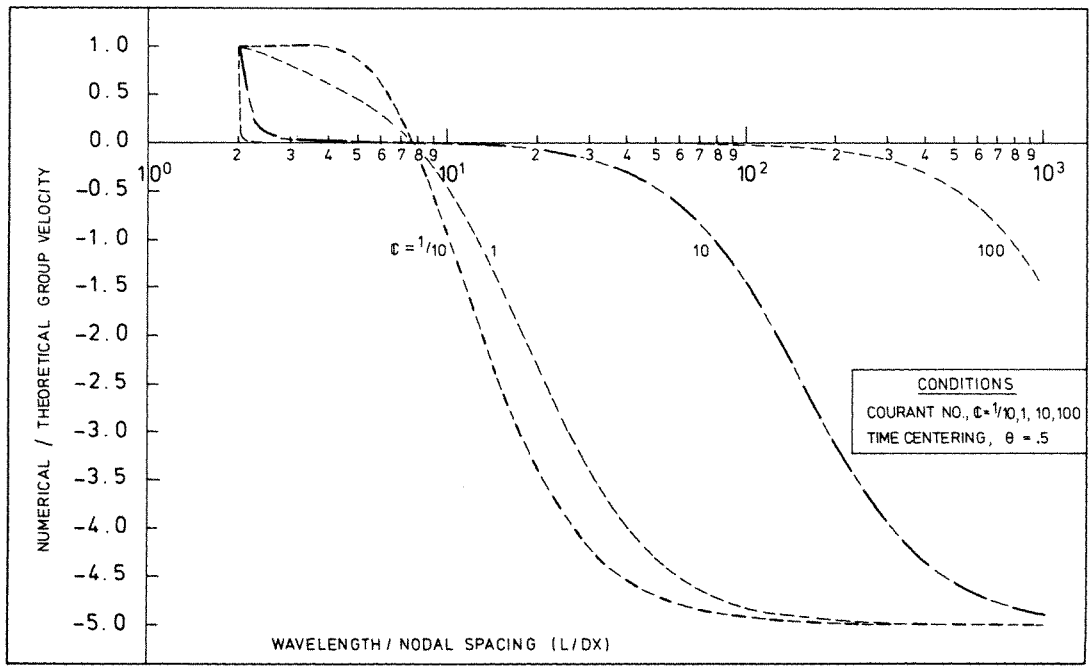

Figure 12. Group-velocity portraits for the spurious computational eigenmodes of Crank–Nicolson quadratic finite elements applied to the shallow water equations: effect of Courant number

Examination of Figure 10 shows that the spurious waves are stationary for $L = 2\Delta x$ and travel upstream in the wrong direction up to a rate of five times too fast for very long waves! These spurious waves are also considerably damped relative to the continuum wave, even at low Courant numbers and with $\theta = 0{\cdot}6$, the scheme's linear stability is guaranteed. At the higher Courant number of 10, it is seen that there is significant (and probably intolerable) damping of the physical mode. However, for wavelengths between $70\Delta x$ and $350\Delta x$, the spurious modes are damped to about 10 per cent of their initial value (a desirable property) after only one continuum wave period.

The numerical group velocity ratio (R) is found by applying equation (33) to equation (44). The calculations are long and are not repeated here (see Reference 6), but the results for the physical and spurious computational modes are plotted in Figures 11 and 12, respectively.

It can be seen that the group velocity portraits are somewhat similar to the phase velocity portraits in Figure 10 and that the quadratic finite element scheme models the phase speed better than the group velocity (as do linear finite elements). It is also evident that in the physical eigenmode, the $2\Delta x$ waves have a group velocity that is five times too large and in the *wrong* direction. In the case of the spurious eigenmode however, the $2\Delta x$ waves are predicted to behave identically with the continuum waves.

Numerical experiments were also carried out for the quadratic elements at a Courant number of 1 and for wavelengths of $2\Delta x$, $4\Delta x$ (not shown) and $8\Delta x$. Typical results are shown in Figures 13 and 14.

The behaviour of the longer waves, $4\Delta x$ and $8\Delta x$, was found to be predicted quite well by the group velocity approach. However, the shortest wavelengths ($2\Delta x$) exhibited a rather odd behaviour. The wave group was found to move forward in the same manner as predicted by the spurious eigenmode whereas the physical mode was predicted to move *backwards* at five times the wave speed. In addition, the wave packet was found to oscillate about mean water level between odd and even time levels, see Figure 13. Additional experiments with different initial conditions were also performed[6] but did not succeed in activating the physical eigenmode.

Other numerical schemes

In view of the general agreement found between the behaviour of the numerical experiments and the group velocity predictions, it was decided to investigate the behaviour of other well known finite difference methods and to compare their behaviour with the linear finite element approach as applied to equation (3) and also to the second order wave equation

$$\frac{\partial^2 u}{\partial t^2} - c^2 \frac{\partial^2 u}{\partial x^2} = 0 \tag{45}$$

which results from the combination of equations (1) and (2) after neglecting the non-linear terms.

Tables I to IV show the results of the group velocity analysis for a selection of the schemes investigated. (Further details are contained in Reference 6).

Figure 15 shows the results of the group velocity analysis at a Courant number equal to $\frac{1}{2}$ applied to two implicit numerical schemes (Crank–Nicolson finite difference and linear finite elements) and two explicit schemes (leap-frog finite difference and linear finite elements). It is interesting that for the two finite element schemes, the group velocity is zero or negative for wavelengths less than $3\Delta x$ but for the finite difference schemes, the corresponding wavelength is $4\Delta x$. Also, the finite element schemes perform worse as far as group velocity is concerned, for those wavelengths between $2\Delta x$ and about $2{\cdot}75\Delta x$, but are better for all wavelengths greater than about $2.75\Delta x$.

Finally in Figure 16, the group velocity performance curves are presented for two numerical schemes contained in Table IV at a Courant number equal to $\frac{1}{2}$ applied to the second order wave

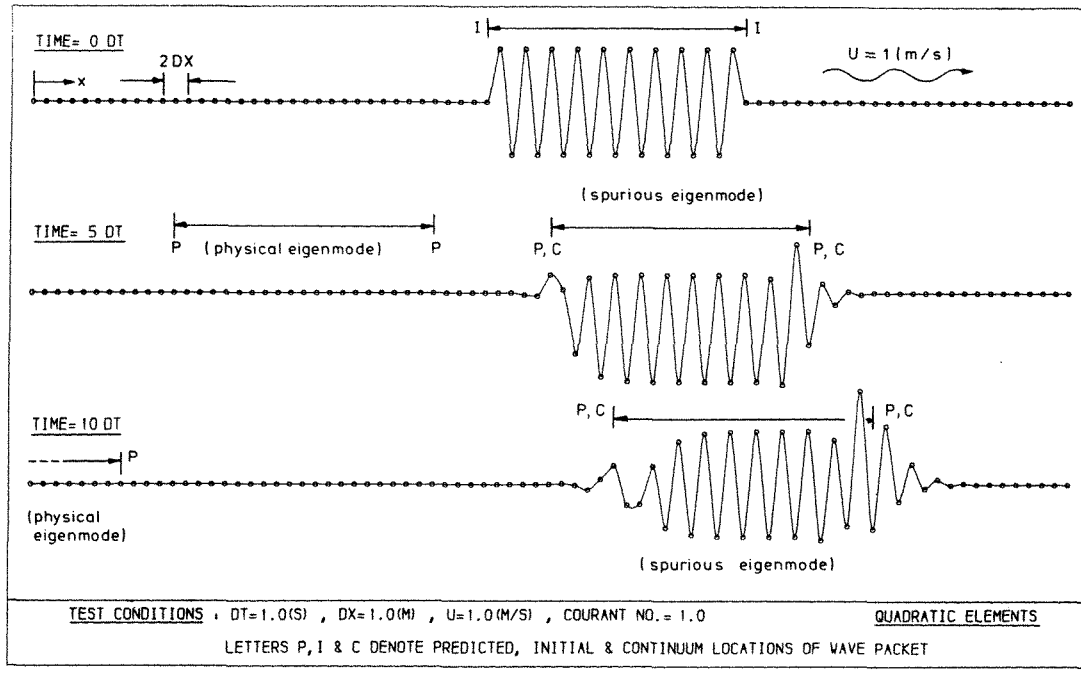

Figure 13. Time evolution of a wave packet made up of waves of wavelength $L = 2\Delta x$

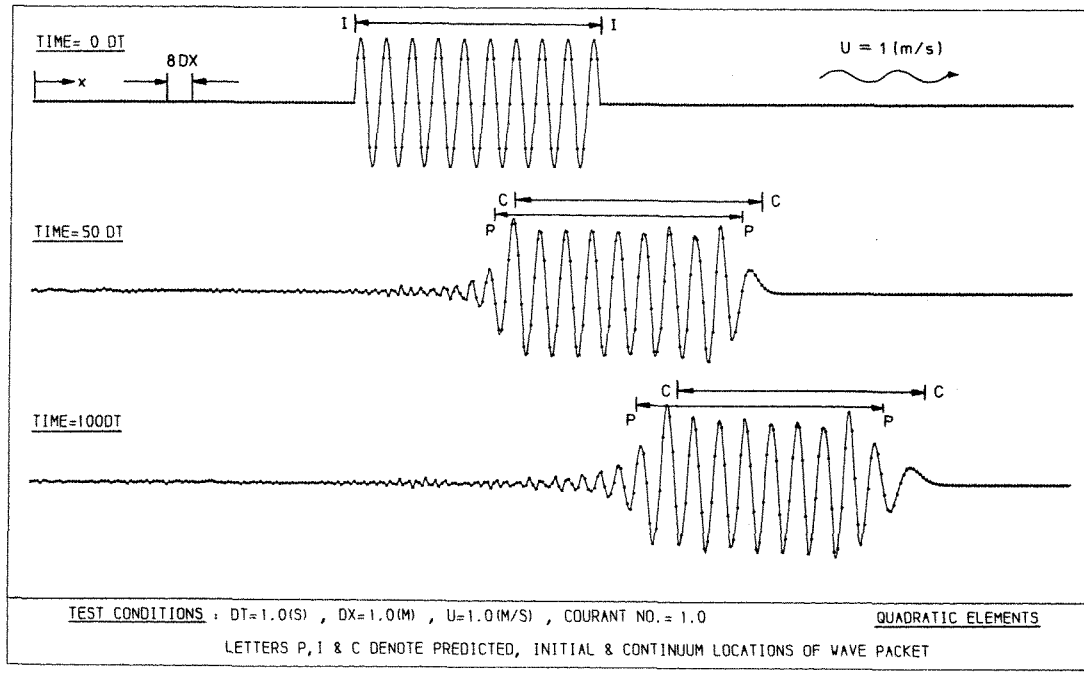

Figure 14. Time evolution of a wave packet made up of waves of wavelength $L = 8\Delta x$

Table I. Numerical/theoretical group velocity (R) for various finite difference schemes when applied to $\partial u/\partial t + c(\partial u/\partial x) = 0$: $\mathbb{C}$ = Courant number and $\gamma = \sigma\Delta x$

NUMERICAL SCHEME	DISCRETE EQUATIONS	EIGENVALUE (λ), $\lvert\lambda\rvert$	STABILITY CONDITION	NUMERICAL GROUP VELOCITY / THEORETICAL GROUP VELOCITY (R)
Backward Differences 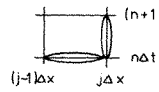	$\left(\frac{u^{n+1}-u^n}{\Delta t}\right)_j + c\left(\frac{u_j - u_{j-1}}{\Delta x}\right)^n = 0$	$\lambda = 1 + \mathbb{C}(\cos\gamma - 1) - i\,\mathbb{C}\sin\gamma$ $\lvert\lambda\rvert = 1 - 2\mathbb{C}(1-\mathbb{C})(1-\cos\gamma)$	$\mathbb{C} \leq 1$	$R = \frac{(1-\mathbb{C})\cos(\gamma) + \mathbb{C}}{[1+\mathbb{C}(\cos\gamma-1)]^2 + [\mathbb{C}\sin\gamma]^2}$
Lax-Friedrichs Finite Difference 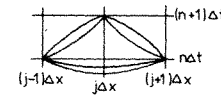	$\frac{u_j^{n+1} - \frac{1}{2}(u_{j+1} + u_{j-1})^n}{\Delta t}$ $+ c\left(\frac{u_{j+1} - u_{j-1}}{2\Delta x}\right)^n = 0$	$\lambda = \cos\gamma - i\,\mathbb{C}\sin\gamma$ $\lvert\lambda\rvert = \cos^2\gamma + (\mathbb{C}\sin\gamma)^2$	$\mathbb{C} \leq 1$	$R = \frac{1}{\cos^2\gamma + [\mathbb{C}\sin\gamma]^2}$
Lax-Wendroff Finite Difference 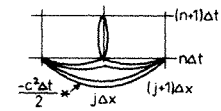	$\left(\frac{u^{n+1}-u^n}{\Delta t}\right)_j + c\left(\frac{u_{j+1}-u_{j-1}}{2\Delta x}\right)^n$ $-\frac{c^2\Delta t}{2}\left(\frac{u_{j+1} - 2u_j + u_{j-1}}{\Delta x^2}\right)^n = 0$	$\lambda = [1 - 2(\mathbb{C}\sin\gamma/2)^2] - i\,\mathbb{C}\sin\gamma$ $\lvert\lambda\rvert = [1 - 2(\mathbb{C}\sin\gamma/2)^2]^2 + [\mathbb{C}\sin\gamma]^2$	$\mathbb{C} \leq 1$	$R = \frac{[1-2(\mathbb{C}\sin\gamma/2)^2]\cos\gamma + [\mathbb{C}\sin\gamma]^2}{[1-2(\mathbb{C}\sin\gamma/2)^2]^2 + [\mathbb{C}\sin\gamma]^2}$

Table II. Numerical/theoretical group velocity (R) for various leap-frog schemes when applied to $\partial u/\partial t + c(\partial u/\partial x) = 0$: $\mathbb{C}$ = Courant number $\gamma = \sigma\Delta x$

NUMERICAL SCHEME	DISCRETE EQUATIONS	EIGENVALUE (λ), $\lvert\lambda\rvert$	STABILITY CONDITION	NUMERICAL GROUP VELOCITY / THEORETICAL GROUP VELOCITY (R)
Leap-Frog (2nd order) Finite Difference 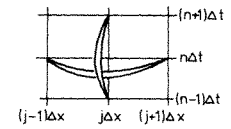	$\left(\frac{u^{n+1}-u^{n-1}}{2\Delta t}\right)_j + c\left(\frac{u_{j+1}-u_{j-1}}{2\Delta x}\right)^n = 0$	$\lambda = \pm\sqrt{1-E^2} - i\,E$ where $E = \mathbb{C}\sin\gamma$ $\lvert\lambda\rvert = 1$	$\mathbb{C} \leq 1$	$R = \frac{\pm\cos(\gamma)}{\sqrt{1-[\mathbb{C}\sin\gamma]^2}}$
Leap-Frog Linear Finite Elements 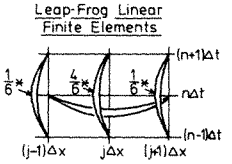	$\frac{1}{6}\left[\left(\frac{u^{n+1}-u^{n-1}}{2\Delta t}\right)_{j-1} + 4\left(\frac{u^{n+1}-u^{n-1}}{2\Delta t}\right)_j + \left(\frac{u^{n+1}-u^{n-1}}{2\Delta t}\right)_{j+1}\right]$ $+ c\left(\frac{u_{j+1}-u_{j-1}}{2\Delta x}\right)^n = 0$	$\lambda = \pm\sqrt{1-E^2} - i\,E$ where $E = \frac{3\mathbb{C}\sin\gamma}{\cos\gamma+2}$ $\lvert\lambda\rvert = 1$	$\mathbb{C} \leq \frac{1}{\sqrt{3}}$	$R = \frac{\pm 3(1+2\cos\gamma)}{(\cos\gamma+2)\sqrt{(\cos\gamma+2)^2 - (3\mathbb{C}\sin\gamma)^2}}$
Leap-Frog (4th order) Finite Difference 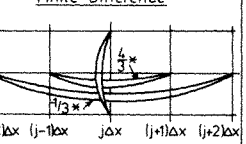	$\left(\frac{u^{n+1}-u^{n-1}}{2\Delta t}\right)_j$ $+ \frac{c}{3}\left[4\left(\frac{u_{j+1}-u_{j-1}}{2\Delta x}\right)^n - \left(\frac{u_{j+2}-u_{j-2}}{4\Delta x}\right)^n\right] = 0$	$\lambda = \pm\sqrt{1-E^2} - i\,E$ where $E = \mathbb{C}(\frac{4}{3}\sin\gamma - \frac{1}{6}\sin 2\gamma)$ $\lvert\lambda\rvert = 1$	$\mathbb{C} \leq .729$	$R = \frac{\pm\frac{1}{3}(4\cos\gamma - \cos 2\gamma)}{\sqrt{1-\mathbb{C}^2\left(\frac{4}{3}\sin\gamma - \frac{1}{6}\sin 2\gamma\right)^2}}$

Table III. Numerical/theoretical group velocity (R) for various finite difference and finite element schemes when applied to $\partial u/\partial t + c(\partial u/\partial x) = 0$: $\mathbb{C}$ = Courant number and $\gamma = \sigma\Delta x$

NUMERICAL SCHEME	DISCRETE EQUATIONS	EIGENVALUE (λ), $\lvert\lambda\rvert$	STABILITY CONDITION	NUMERICAL GROUP VELOCITY / THEORETICAL GROUP VELOCITY (R)
Preissman's Box Scheme 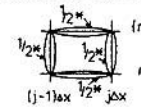	$\frac{1}{2}\left(\frac{u^{n+1}-u^n}{\Delta t}\right)_{j-1} + \frac{1}{2}\left(\frac{u^{n+1}-u^n}{\Delta t}\right)_j + \frac{C}{2}\left(\frac{u_j - u_{j-1}}{\Delta x}\right)^{n+1} + \frac{C}{2}\left(\frac{u_j - u_{j-1}}{\Delta x}\right)^n = 0$	$\lambda = \frac{1 - i\mathbb{C}E}{1 + i\mathbb{C}E}$ where $E = \mathbb{C}\tan\gamma/2$ $\lvert\lambda\rvert = 1$	unconditionally stable	$R = \frac{1}{\cos^2(\gamma/2) + [\mathbb{C}\sin(\gamma/2)]^2}$
Crank-Nicolson Finite Difference 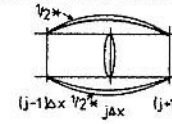	$\left(\frac{u^{n+1}-u^n}{\Delta t}\right)_j + \frac{C}{2}\left(\frac{u_{j+1}-u_{j-1}}{2\Delta x}\right)^{n+1} + \frac{C}{2}\left(\frac{u_{j+1}-u_{j-1}}{2\Delta x}\right)^n = 0$	$\lambda = \frac{1 - i\mathbb{C}E}{1 + i\mathbb{C}E}$ where $E = \mathbb{C}/2\sin\gamma$ $\lvert\lambda\rvert = 1$	unconditionally stable	$R = \frac{\cos\gamma}{1 + (\mathbb{C}/2\sin\gamma)^2}$
Crank-Nicolson Linear Finite Element 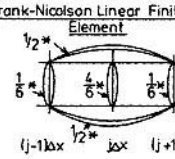	$\frac{1}{6}\left[\left(\frac{u^{n+1}-u^n}{\Delta t}\right)_{j-1} + 4\left(\frac{u^{n+1}-u^n}{\Delta t}\right)_j + \left(\frac{u^{n+1}-u^n}{\Delta t}\right)_{j+1}\right] + \frac{C}{2}\left(\frac{u_{j+1}-u_{j-1}}{2\Delta x}\right)^{n+1} + \frac{C}{2}\left(\frac{u_{j+1}-u_{j-1}}{2\Delta x}\right)^n = 0$	$\lambda = \frac{1 - i\mathbb{C}E}{1 + i\mathbb{C}E}$ where $E = \frac{3/2\,\mathbb{C}\sin\gamma}{\cos\gamma + 2}$ $\lvert\lambda\rvert = 1$	unconditionally stable	$R = \frac{3(1 + 2\cos\gamma)}{(\cos\gamma+2)^2 + (3\mathbb{C}/2\sin\gamma)^2}$

equation. The region of interest is contained in the $2\Delta x$ to about $10\Delta x$ wavelength range. It is seen that the finite elements propagate the wave group too rapidly whereas the finite difference scheme propagates them too slowly, but that both schemes propagate the energy in the correct direction for all wavelengths except for the stationary wave packets consisting of $2\Delta x$ waves. It is interesting to note that it was the better damping and phase propagation characteristics that lead Lynch and Gray[7] to base their water circulation model on the second order wave equation, rahter than the shallow water equations.

Table IV. Numerical/theoretical group velocity (R) for the finite difference and finite element schemes when applied to $\partial^2 u/\partial t^2 - c^2(\partial^2 u/\partial x^2) = 0$: $\mathbb{C}$ = Courant number and $\gamma = \sigma\Delta x$

NUMERICAL SCHEME	DISCRETE EQUATIONS	EIGENVALUE (λ), $\lvert\lambda\rvert$	STABILITY CONDITION	NUMERICAL GROUP VELOCITY / THEORETICAL GROUP VELOCITY (R)
Wave Equation Finite Difference 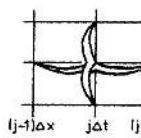	$\left(\frac{u^{n+1} - 2u^n + u^{n-1}}{\Delta t^2}\right)_j - c^2\left(\frac{u_{j+1} - 2u_j - u_{j-1}}{\Delta x^2}\right)^n = 0$	$\lambda^{\pm} = E \mp i\sqrt{1-E^2}$ where $E = 1 - 2(\mathbb{C}\sin\gamma/2)^2$ $\lvert\lambda^{\pm}\rvert = 1$	$\mathbb{C} \leq 1$	$R = \frac{\cos\gamma/2}{\sqrt{1-(\mathbb{C}\sin\gamma/2)^2}}$
Wave Equation Linear Finite Elements 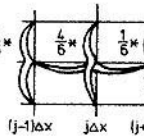	$\frac{1}{6}\left[\left(\frac{u^{n+1}-2u^n+u^{n-1}}{\Delta t^2}\right)_{j-1} + 4\left(\frac{u^{n+1}-2u^n+u^{n-1}}{\Delta t^2}\right)_j + \left(\frac{u^{n+1}-2u^n+u^{n-1}}{\Delta t^2}\right)_{j+1}\right] - c^2\left(\frac{u_{j+1} - 2u_j + u_{j-1}}{\Delta x^2}\right)^n = 0$	$\lambda^{\pm} = E \mp i\sqrt{1-E^2}$ where $E = 1 + \frac{3\mathbb{C}^2(\cos\gamma - 1)}{\cos\gamma + 2}$ $\lvert\lambda^{\pm}\rvert = 1$	$\mathbb{C} \leq \sqrt{\frac{1}{3}}$	$R = \frac{9\mathbb{C}\sin\gamma}{(\cos\gamma+2)\sqrt{(\cos\gamma+2)^2 - [\cos\gamma+2-3\mathbb{C}^2(\cos\gamma-1)]^2}}$

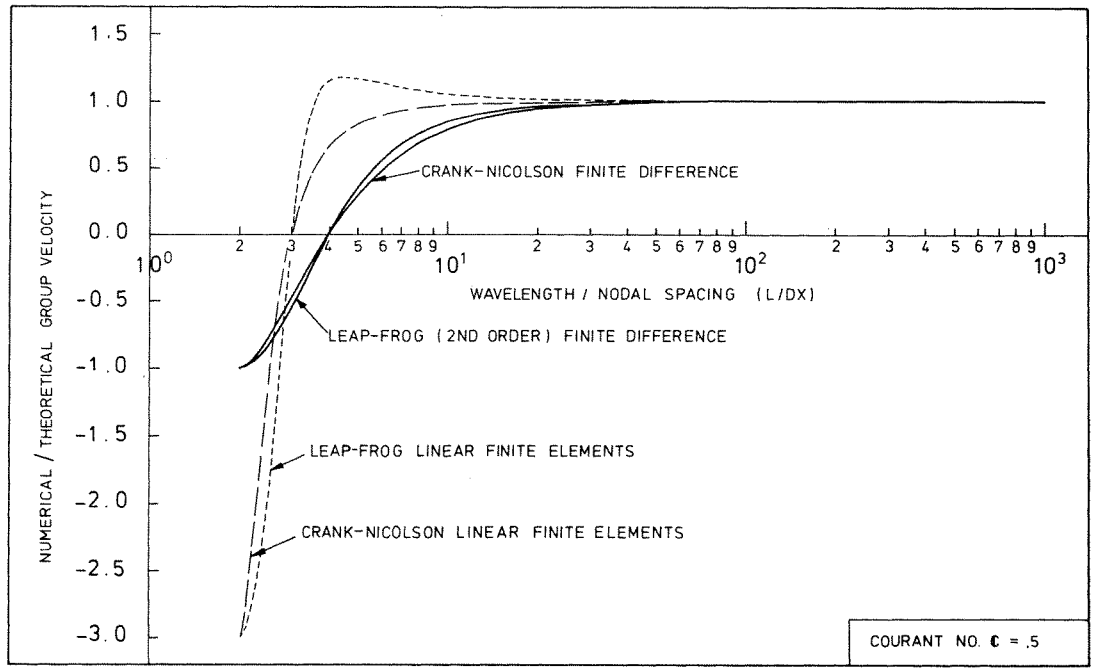

Figure 15. Group velocity portraits of two finite difference schemes (leap-frog and Crank–Nicolson) and their finite element counterparts when applied to $\partial u/\partial t + c(\partial u/\partial x) = 0$

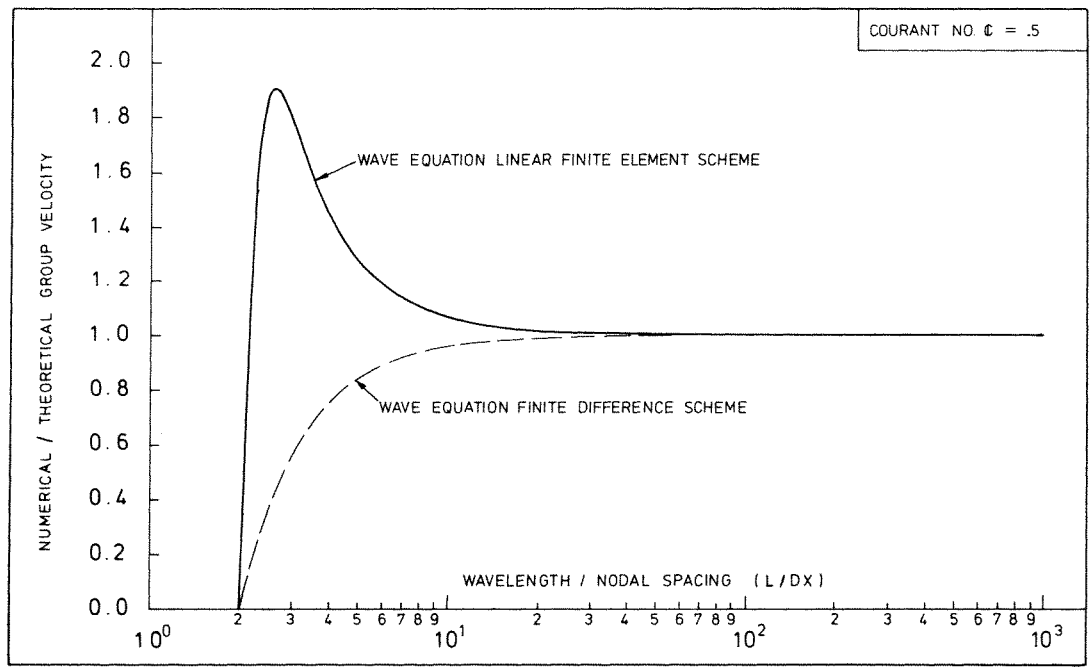

Figure 16. Group velocity portraits of the wave equation finite difference scheme and its finite element counterpart applied to $U_{,tt} - c^2 U_{,xx} = 0$

CONCLUSIONS

The group velocity portrait (equations (33) or (34)) of a numerical scheme supplements the well known wave amplitude and phase velocity portraits used by analysts to assess the accuracy of a numerical scheme. It also provides some understanding as to what may otherwise appear as puzzling behaviour for a numerical scheme—especially with regard to the disappearance or appearance of short wavelength oscillations and their sometimes rapid, apparent propagation counter to that occurring in the continuum. In the case of the linear finite elements discussed in this paper, this happens where the analysis predicts a zero phase velocity—i.e. stationary waves.

Group velocity portraits were calculated for linear and quadratic elements used in conjunction with Crank–Nicolson finite differencing in time. The results showed that the group velocity representation in these numerical schemes was worse than the phase velocity and that energy propagation associated with the short wavelengths was particularly bad, being 3 times (for linear elements) or even 5 times (for quadratic elements) too fast in the wrong (i.e. upstream) direction.

The superiority of the quadratic element over the linear element, as a transporter of energy, may be real over all wavelengths, in spite of the results of the group velocity portraits (Figures 11 and 12). This is due to the existence of a computational mode (Figure 12) for the quadratic elements, which has perfect energy propagation for $2\Delta x$ wavelengths and a better performance than the physical eigenmode for wavelengths up to $4\Delta x$. The numerical experiments conducted did not succeed in activating the worse behaved physical eigenmode for wavelengths between $2\Delta x$ and $4\Delta x$, in spite of varied initial conditions. Thus it may be that the quadratic elements' performance succeeds in getting the best of both worlds. (i.e. the best of the physical and computational eigenmodes).

By examining the group velocity portraits for a diversity of numerical schemes, the results reinforce the fact that it is not sufficient to assess a numerical scheme by only inspecting the truncation error.

In numerical schemes that are free of amplitude errors ($P = 1$), it is possible to have perfect reproduction of the group velocity only under special conditions, such as Courant no. $= 1$.

The behaviour of the group velocity of a numerical scheme has important implications for wave modelling within the wave period using the Boussinesq equations, as described by Abbott *et al.*[8], in contrast to modelling waves using a time-averaged approach via radiation stresses. The present results suggest that a good spatial resolution is even more vital if the Boussinesq approach is to be used as the basis of future models.

ACKNOWLEDGEMENTS

This work has been supported in part by the North West Consortium for Marine Technology and its help is gratefully acknowledged. We also wish to thank our colleague, Ralph Penoyre for some helpful discussions on the above work.

REFERENCES

1. J. J. Leendertse, 'Aspects of a computational model for long-period water-wave propagation', Rand Corp., Santa Monica, *RM-5294-PR*, May 1967.
2. R. J. Sobey, 'Finite difference schemes compared for wave deformation characteristics in mathematical modelling of two-dimensional long wave propagation', *Technical Memorandum No. 32*, US. Army Corps of Engineers, Coastal Engineering Research Centre, October 1970.
3. R. Grotjahn and J. J. O'Brien, 'Some inaccuracies in differencing hyperbolic equations', *Mon. Wea. Rev.*, **104**, 180–194 (1976).
4. L. J. F. Broer, 'On the propagation of energy in linear conservative waves', *Applied Sci. Research*, A2, Martinus Nijhoff, 1951.

5. G. B. Whitham, 'Non-linear dispersion of water waves', *J. Fluid Mech.*, **27,** 399–412 (1967).
6. B. O'Connor and B. Cathers, 'Considerations of group velocity in some numerical schemes', *Department of Civil Engineering Report No. HHS/83/01*, University of Manchester, July 1983.
7. D. R. Lynch and W. G. Gray, 'A wave equation model for finite element tidal computations', *Computers & Fluids*, **7,** 207–228, (1979).
8. M. B. Abbott, H. M. Peterson and O. Skovgaard, 'On the numerical modelling of short waves in shallow water', *J. Hydraulic Research*, **16,** 173–203 (1978).